Hindawi
Journal of Food Biochemistry
Volume 2023, Article ID 5553926, 17 pages
https://doi.org/10.1155/2023/5553926

Research Article

Efficacy for Bone Deterioration in Mice with Osteoporosis and Pharmaceutical Properties of a Novel Compound Calcium Carbonate Granule

Kun Ma, Jialuo He, Huimin Yuan, Jiayu He, and Ming Xiang

Department of Pharmacology, School of Pharmacy, Tongji Medical College, Huazhong University of Science and Technology, Wuhan, Hubei, China

Correspondence should be addressed to Ming Xiang; xiangming@tjmu.edu.cn

Received 3 February 2023; Revised 10 May 2023; Accepted 15 May 2023; Published 15 June 2023

Academic Editor: Jae Young Je

Osteoporosis (OP) has been a global health concern, and calcium supplements are still an effective method to relieve the disease. In this study, we investigated the pharmaceutical properties, antiosteoporosis, and adverse effects of a novel calcium supplement named compound calcium carbonate granule (CCCG). The dissolution rate, stability of vitamin D_3, and drug permeability of the calcium supplements were explored. And the osteoporosis was constructed in mice with retinoic acid (100 mg/kg/d) for 21 days, and orally treated with CCCG (0.34, 0.68, and 1.36 g/kg/d) for 36 days to evaluate the efficacy against osteoporosis and the occurrence of kidney stones. The results showed that CCCG exhibited higher dissolution rate and better vitamin D_3 stability than the standard calcium carbonate granule. CCCG also displayed more absorption in Caco-2 cell model. On the other hand, CCCG alleviated the deterioration in femur microstructure and oxidative stress in the liver and kidney, and increased the expression of bone metabolic markers. CCCG also exhibited lower risk of nephrolithiasis than the commercial calcium carbonate granule. In summary, from the perspectives of both pharmaceutics and efficacy, we illustrated the profiles of an intriguing calcium supplement, which could possibly be an alternative of commonly used ones. *Practical Application.* Calcium carbonate is widely used to supplement calcium, primarily because of its high calcium load, low cost, and good efficacy. Now, we provided a new calcium supplement named CCCG, which was prepared by inclusion and complexation techniques. Vitamin D_3 in CCCG was made into vitamin D-β-cyclodextrin inclusion complex by inclusion technology, which improved the stability of vitamin D_3. And calcium carbonate was converted to a water-soluble calcium citrate complex via complexation techniques to accelerate the release of calcium ions and minimize the risk of kidney stone formation. From the perspective of both pharmaceutics and efficacy, we illustrated the profiles of an intriguing calcium supplement, which could possibly be an alternative for the supplemental and preventive treatment of osteoporosis.

1. Introduction

Characterized by low bone mineral density (BMD) and deterioration of microstructure in the bone tissue [1], osteoporosis and osteoporosis fracture are great health concerns globally, especially for the aged and postmenopausal population. A report showed that in China, the prevalence of osteoporosis in 2019 in male and female over the age of 50 was estimated at 6.46% and 29.13%, respectively [2]. Though faced with arguments, calcium with vitamin D can still work as an effective choice against BMD decrease [3, 4], a strong predictor of osteoporosis.

Over 99% of the total body calcium is stored in the skeletal system, the reservoir of body calcium [5]. As suggested by the National Institute of Health (NIH) and Institute of Medicine (IOM), daily calcium intake varies according to age groups, but generally ranges from 800 to 1000 mg for adults with a tolerable upper intake level of 2500 mg [6]. However, the worrying fact is that the medium of Chinese dietary calcium intake is only 328.4 mg per day,

though the amount is likely to rise with increasing levels of education, income, and urbanization [7].

Despite the importance mentioned above, up-to-date pharmacologic agents on the current market (e.g., bisphosphonates, receptor activator of nuclear factor kappa-B ligand (RANKL) inhibitors, selective estrogen receptor modulators (SERMs), and parathyroid hormone-related peptide analogues) are facing some drawbacks, such as side effects, unaffordable costs, poor patient compliance, and the inability to fully restore the balance of bone metabolism [8]. For calcium supplements, deficiency in calcium intake could raise the odds of nephrolithiasis [9, 10]. Urine pH could be another risk factor. The prevalence of kidney stone may rise when urine pH is lower than 6.5, which could also affect calcium absorption [11]. Moreover, calcium carbonate, the most commonly used form, requires gastric acid to be digested due to its poor solubility in water [12]. This may lead to indigestion for people of insufficient gastric acid excretion such as kids and the aged [13].

Here, we reported a novel formulation, calcium carbonate compound granules (CCCGs), which could form a complex of calcium carbonate and calcium citrate in water. We selected the conventional calcium supplement named calcium carbonate with vitamin D (CCD) as reference drug and conducted the study of the pharmaceutical properties and adverse effects of CCCG. While in both osteoporosis murine model and in vitro cell assays, we proved CCCG with more efficacy and unique dissolution profiles, and a lower possibility to cause kidney stones.

2. Materials and Methods

2.1. Preparation of CCCG. CCCG was provided by XiMo Pharmaceuticals (H20173214, WuHan, China). CCCG was prepared by applying two pharmaceutical approaches—"complexation" and "inclusion" technologies [14, 15]. First, vitamin D_3 ethanol solution was dripped into β-cyclodextrin solution to form the vitamin-D-β-cyclodextrin inclusion complex via the inclusion technology, which made vitamin D_3 more stable. Meanwhile, calcium carbonate was mixed with citric acid and filling agents to form a water-soluble calcium citrate complex via the complexation technology. Finally, vitamin D_3 and calcium citrate complex were added to the mix in binder ethanol solution and pelleted effervescent agent to acquire CCCG. Excipients used in the process are listed in Table 1. CCD was obtained from LangDi Pharmaceuticals (H20090334, Beijing, China).

2.2. Determination of Particle Size. Malvern Mastersizer 2000 laser particle analyser was used for particle size of CCCG and CCD granules. A certain weight of thoroughly and evenly mixed sample was baked at $(105 \pm 2)^{\circ}$C for 15 minutes to remove moisture. Testing mode was selected as dry method. The shading rate was kept between 7% and 10%. The particle size range of the instrument is 2~3000 nm, and the incident wavelength is 670 nm, with the test temperature at 25°C.

2.3. Determination of Specific Surface Area and Pore Size Distribution. The F-Sorb 2400 nitrogen adsorption specific surface area meter was used to determine the specific surface area and pore size distribution curve of CCCG and CCD. Firstly, the sample was degassed by heating and vacuum pumping to remove adsorbed impurities on the surface. After the sample cools to room temperature, it was backfilled with helium gas. When the helium gas was filled to atmospheric pressure, the sample tube was sealed and weighed to 0.1 mg. Then, the sample was placed in liquid nitrogen to measure the nitrogen adsorption amount of the sample at predetermined pressure points, obtaining the adsorption isotherm. Specific surface area, pore volume, and pore size distribution were calculated from the adsorption isotherm.

2.4. Dissolution Rate and Stability of Vitamin D_3. Release rate was quantified according to Chinese Pharmacopeia 2020, Book 4, Issue 0931, Method 2. The rotator was set at 50 rpm, and release medium was 700 mL chloride hydrate solution (pH = 1). 5 mL samples were taken at 5, 10, 15, 20, 30, 45, 60, 90, and 120 min, the same volume of medium was supplemented after each sampling. Calcium concentration was measured according to Mohammad's reports using a SpectrAA-240FS flame atomic absorption spectroscopy (FAAS) system (Agilent, USA) [16]. Parameters: wavelength: 422.7 nm; hollow cathode lamp current: 10 mA; fuel: air-C_2H_2; fuel flow rate: 2.00 L/min; air flow rate: 13.50 L/min; slit width: 0.5 nm; BGC-D2 was used as background check method. To establish the standard curve, calcium standard solution of 0, 0.5, 1.0, 2.0, and 3.0 mg/mL was prepared and measured absorption at 422.7 nm.

Vitamin D_3 stability was evaluated according to Rakmai's report [17]. A UV light (G15T8, Philips) was adopted. Samples of standard vitamin D_3 (Shuangjing Pharmacy, China) and CCCG containing 800 IU were radiated under UV light at the distance of 20 cm. Samples were taken at the timing of 0, 5, 10, 15, 20, 30, 45, 60, 90, and 120 min. Vitamin D_3 measurement was carried out with high-performance liquid chromatography (HPLC) according to Chinese Pharmacopeia 2020, Book 4, Issue 0512. UV-detector at 265 nm was used. C18 column (250 mm × 4.6 mm, 5 μm, OSAKA SODA Co., Ltd., Osaka, Japan) was used as a stationary phase. The mobile phase was methanol: acetonitrile: water = 50 : 50 : 2 (v/v).

2.5. In Vitro Drug Permeability. Human colon carcinoma cell line Caco-2 (Cell Bank of Chinese Academy of Science, Shanghai) was grown in high glucose Dulbecco's Modified Eagle Medium (DMEM; Hyclone) containing $_{L}$-glutamine, supplemented with 15% (v/v) fetal bovine serum (FBS; PAN) and 1% (v/v) antibiotics (Hyclone; 100 U/mL penicillin and 100 U/mL streptomycin). Caco-2 cells were seeded on transwell inserts (polyester membrane, 0.4 μm pore size, Corning Costar Corp, NY, USA). Cells were maintained for 21 days and consequently reached confluence to differentiate into a monolayer. The integrity of Caco-2 cell monolayer was evaluated using fluorescein sodium (Aladdin, China).

Table 1: Excipients used in CCCG manufacturing.

Excipients	Name	Proportion (compared to calcium carbonate)
Effervescent agents	Citric acid, malic acid, tartaric acid, or their combination	1~2
Binders	PVP, HPMC, or combination	0.01~0.4
Fillers	Lactose, sorbitol, mannitol, MCC, icing sugar, or their combination	15~40% total mass
Flavouring agents	Aspartame, sucrose, stevioside, sorbitol, or their combination	1~20% total mass

To imitate the digestion process, the granules were dissolved in 50 mL HCl solution (pH = 2) and shaked for 30 min; then, we raised pH back to 7 using $NaHCO_3$. Before permeability assay, the medium was removed, and cells were washed with warm Hanks' Balanced Salt Solution (HBSS) for three times. The last wash was reserved for baseline detection. 500 μL of CCCG or CCD solution was added in apical chambers and 1500 μL HBSS in basolateral sides. Assays were done in triplet. Both apical and basolateral solution were collected at 20, 40, and 60 min, and the chambers were refilled with HBSS. Then, calcium concentration was measured as mentioned above. To compare the permeability rate of CCCG and CCD, apparent permeability factor (P_{app}) was calculated according to the following formula:

$$P_{app} = \frac{(dQ/dt)}{(A \times C0)}, \quad (1)$$

where dQ/dt is the amount of product present in the basal (A-B) or apical (B-A) compartment as a function of time (μg/min), A is the area of transwell polyester membrane (cm^2), C0 is the initial concentration of the product applied in the apical (A-B) or basal (B-A) compartment (μg/mL).

2.6. Animal Experiments

2.6.1. Osteoporosis Model Establishment and Experimental Design. The animal study was approved by the Institutional Animal Care and Use Committee of Tongji Medical College, Huazhong University of Science and Technology ((2018) IACUC number: 2671). A total of 52 female 11-week-old BALB/c mice were purchased from Jiangsu Jicui Laboratory Animal Technology Co., Ltd. (China). Mice were group-housed at the Experimental Animal Center of Tongji Medical College (Huazhong University of Science and Technology) in specific-pathogen-free (SPF) cages, and maintained under 26°C and 12 h light/dark cycle. Mice were fed ad libitum with chow diet and water. Mice were allowed to acclimate for 1 week before further treatments.

Mice were treated with saline (0.1 mL/d, $n = 12$) or retinoic acid (RA, 100 mg/kg/d, $n = 40$) by gavage [18]. After 21 days of RA administration, five mice of different treatment were randomly selected to confirm model establishment. The remaining mice in the normal ($n = 7$) and model groups ($n = 35$) were given the following treatments: saline-treated mice continued to be given the same treatment as control groups. RA-treated mice were randomly grouped ($n = 7$) and treated by oral gavage with normal saline, CCCG (0.34, 0.68, and 1.36 g/kg/d), and CCD (0.9 g/kg/d) for 36 days. CCD mice were administered according to a guidance released by the US Food and Drug Administration in 2005, "Estimating the Maximum Safe Starting Dose in Initial Clinical Trials for Therapeutics in Adult Healthy Volunteers." Weights of the mice were recorded during the process.

The liver, spleen, and kidney as well as the tibia and femur were dissected. Lengths and diameters of the femurs were measured. Weights of the liver, spleen, kidney, left tibia, and femur were quantified; data were used to calculate organ indexes using the following formula: organ index- = mean organ weight (mg)/mean body weight (g) [19].

2.6.2. Biochemical Assays. Blood samples were collected from each group of mice and was centrifuged at 6000 rpm/min, 4°C for 10 min; serum was stored at −80°C before use. Serum calcium and phosphorus concentration were quantified using corresponding kits (Zhenke, China); BALP (bone alkaline phosphatase), PINP (procollagen type I N-terminal propeptide), and OPG (osteoprotegerin) levels were quantified according to the instructions of corresponding enzyme-linked immunosorbent assay (ELISA) kits (Zhenke, China).

The liver and kidney tissues of mice were ground and centrifuged to collect the supernatant. Tissue MDA (malondialdehyde), SOD (superoxide dismutase), and CAT (catalase) levels were quantified according to the instructions of the corresponding ELISA kits (Solarbio, China).

2.6.3. Micro-CT Analysis. Right femurs from mice were fixed in 4% polyethene for 1 week. Samples were fit vertically in the container and scanned for microstructure (SkyScan 1176, Bruker; Kontich, Belgium; 58 kV and 431 μA; 0.5 mm aluminum; exposure time: 1000 ms; image pixel size: 9.00 μm; rotation angle and range: 0.30° over 180° rotation; frame averaging: OFF). We used NRecon 1.7.4.6 (Bruker, Kontich, Belgium) to reconstruct raw images into 3-dimensional images. CTAn and CTVox (SkyScan) were used to calculate structural indices. An area of 0.5 mm away from the femoral growth plates was set as regions of interest (ROI). Trabecular bone volume (BV/TV), trabecular thickness (Tb.Th), trabecular separation (Tb.Sp), trabecular number (Tb.N), and trabecular pattern factor (Tb.Pf) were calculated.

2.6.4. Biomechanical Parameter Analysis. After the micro-CT scan was completed, the right femur was tested for biomechanical properties using a servohydraulic test system

(MTS acumen3, USA) at the speed of 0.01 mm/s. The peak load was recorded and used to calculate the stiffness, maximum load, maximum deflection, and fracture energy. These parameters were derived from the displacement and force measurements.

2.6.5. Hematoxylin and Eosin (H&E) Staining. Left femurs were isolated for histological analysis. In brief, bone samples were fixed with 4% paraformaldehyde, then decalcified and dehydrated, finally embedded in paraffin. Samples were cut in 5 μm slices and then dewaxed by xylene and alcohol in the order of 100, 95, 75, and 50%. Slices were soaked in distilled water and stained with H&E according to the standard scheme. Leica DMI6000 B (Leica, German) was used to capture fields with positive staining.

2.6.6. The pH and Calcium Concentration Measurement of Mice Urine. Urine of mice in 24 h in each group was collected centrifuged. The supernatant was frozen at −80°C. The pH meter detected the acid-base property of mice's urine. Calcium concentration was measured using a SpectrAA-240FS FAAS system, as shown in Method 2.4.

2.7. Cell Culturing and Assays. HOS (human osteosarcoma) cells were obtained from the Department of Clinical Pharmacy, Union Hospital, Wuhan. Cells were grown in minimum essential medium α (α-MEM, Hyclone) supplemented with 10% (v/v) FBS (Gibco, US) and 1% (v/v) antibiotics. When cells reached 80% confluence, replace the medium with α-MEM including 10 mM β-sodium glycerophosphorus, 100 nM dexamethasone, and 50 μg/mL ascorbic acid. Cells were treated with CCCG low (50 μg/mL), medium (100 μg/mL), and high (200 μg/mL) doses and CCD (88 μg/mL).

HOS cells were plated at the density of 5×10^4 cells/mL into 96-well plates (200 μL medium per well) with five replicates. Cells were then treated with different concentrations of CCCG. After incubation for 48 h, cell viability was measured using CCK8 assay according to manufacturer's instruction. After differentiation and administration, alkaline phosphatase (ALP) activity was measured by ALP kits (Beyotime, China). ALP staining was conducted with 5-bromo-4-chloro-3-indolyl phosphate/nitrotetrazolium blue chloride (BCIP/NBT) dye (Beyotime, China), and the stained cells were observed by optical microscopy.

Fourteen days after treatment, HOS cells were fixed with 4% polyoxymethylene for 10 min and then dyed with 1% Alizarin red S-Tris-HCl (Sigma-Aldrich, US; pH = 4.2) staining solution for 30 min. Cells were observed and photographed with an optical microscope. For quantitative analysis, cells were washed with cetylpyridinium chloride monohydrate for 30 min at room temperature and transferred to a 96-well plate to measure the absorbance at 550 nm using a microplate reader.

2.8. Real-Time Quantitative Polymerase Chain Reaction (RT-qPCR). Total RNA was isolated from HOS cells with Trizol (Invitrogen, Carlsbad, CA) as per kit directions, and 2 μg of RNA and reverse transcriptase per tube were used as templates to form cDNA using the PrimeScript™RT kit (TaKaRa, Japan). Subsequently, the cDNA was amplified via incubation at 95°C for 5 min, with a thermal cycle profile of 40 cycles of denaturation at 95°C for 10 s, annealing at 55–60°C for 20 s, and extension at 72°C for 30 s. Normalization of relative gene expression was done with levels of endogenous GAPDH that served as control and calculated using the $^{\Delta\Delta}$Ct method. Gene-specific primer sequences used are listed in Table 2.

2.9. Western Blotting. After forty-eight hours of treatment, total protein of HOS was extracted with radio immunoprecipitation assay (RIPA) lysis buffer containing proteinase and phosphatase inhibitors (ABP, USA). Protein concentration was quantified with the bicinchoninic acid (BCA) protein assay method (ABP, USA). The loading amount of protein applied to each slot was 20 μg. In brief, the protein lysates were separated on 10–15% sodium dodecyl sulfate-polyacrylamide gels by electrophoresis (SDS-PAGE) and transferred onto polyvinyl difluoride (PVDF) membranes. Membranes were blocked with 5% bovine serum albumin (BSA) for 1 h at 37°C, followed by an overnight incubation with the corresponding primary antibodies (1 : 1000 diluted in TRIS-buffered saline and tween (TBST) according to the instructions) at 4°C with gentle shaking. After washing with TBST, the membrane was incubated at room temperature for 1 hour with anti-rabbit IgG ($H + L$) (DyLight™ 680 Conjugate, #5366) or anti-mouse IgG ($H + L$) (DyLight™ 800 Conjugate, #5257) secondary antibodies (1 : 10000 in TBST; Cell Signaling Technologies, USA). Blots were then visualized with Odyssey Infrared Imaging System (LI-COR Biosciences, Lincoln, NE, USA). Antibodies used were anti-β-catinien (ab32572, Abcam, USA) and anti-runt-related transcription factor 2 (RUNX2) (ab326639, Abcam, USA).

2.10. Statistical Analysis. Statistical analysis was performed with the GraphPad Prism 6.0 and SPSS 20.0 software for Windows. All data were expressed as the mean ± SEM. The differences between multiple groups were analysed for statistical significance using one-way analysis of variance (ANOVA), followed by the least significant difference (LSD) method for post hoc analysis. The differences between the two groups were examined for statistical significance using the unequal variance and two-tailed Student's t-test. The results were considered to be statistically significant if $P < 0.05$.

Table 2: RT-qPCR primers sequences for related genes of HOS.

Genes	Forward primer sequence	Reverse primer sequence
ALP	ACCTCGTTGACACCTGGAAG	CCACCATCTCGGAGAGTGAC
COL-I	GACTGCCAAAGAAGCCTTGCC	TTCCTGACTCTCCTCCGAACCC
RUNX2	TTACTTACACCCCGCCAGTC	TATGGAGTGCTGCTGGTCTG
BMP2	ACTCGAAATTCCCCGTGACC	CCACTTCCACCACGAATCCA
OTC	GACTGTGACGAGTTGGCTGA	CTGGAGAGGAGCAGAACTGG
OPG	GAACCCCAGAGCGAAATACA	CGCTGTTTTCACAGAGGTCA
OPN	CTCCATTGACTCGAACGACTC	CAGGTCTGCGAAACTTCTTAGAT
GAPDH	GCACCGTCAAGGCTGAGAAC	ATGGTGGTGAAGACGCCAGT

3. Results

3.1. Dissolution Rate of CCCG and the Stability of Vitamin D_3. Quantity of vitamin D_3 in CCCG reduced statistically slower than vitamin D_3 standard in 20 and 90 min (Figure 1(e)). At 60 min, the concentration of vitamin D_3 in CCCG was higher than CCD ($0.74 \pm 0.09\,\mu$g/mL versus $0.33 \pm 0.03\,\mu$g/mL, $^*P < 0.05$), suggesting that the inclusion procedure of vitamin D_3 provided good protection against decomposition. Dissolution rate of CCCG and CCD at each timing was quantified. CCCG exhibited a better dissolution profile, taking effect in a shorter time. As Figure 1(c) showed, CCCG exhibited superior stabilization rate between 5 and 30 min. On the other hand, at 30 min, the dissolution rate of CCCG reached $76.77 \pm 3.15\%$ while CCD reached only $64.47 \pm 2.97\%$. And from here a better clinical potential can be anticipated.

To address the impact of particle size and specific surface area on the dissolution behaviour of CCCG and CCD, we conducted further experiments to measure their particle size, specific surface area, and pore size distribution. The results obtained from Malvern Mastersizer 2000 laser particle analyser are presented in Table 3 and Figure 1(a). The particle size of CCCG granules was smaller than that of CCD, which was determined by the value of D (4, 3). The diameter distribution of CCCG was also smaller than that of CCD, as indicated by d (0.1), d (0.5), and d (0.9). The specific surface area of CCCG was $0.080 \pm 0.01\,m^2/g$, and the pore volume was $(4.3 \pm 0.6) \times 10^{-5}\,cm^3/g$, with a pore diameter of less than 2.50 nm. In comparison, the specific surface area of CCD was slightly higher, as shown in Table 4, without significance. Although the CCD particles are larger in size, their specific surface area may still be higher due to factors such as more small pores or the shape of particles, which can provide more surface area on larger particles. To minimize the effect of particle size and specific surface area on dissolution behaviour, we further ground CCCG and CCD into fine fractions to reach uniform particle size and surface area and detected the release rate of calcium ions. Table 5 shows the particle size and BET specific surface area of CCCG and CCD granules after grinding. The results showed that CCCG exhibited a good stable rate between 5–20 minutes. On the other hand, at 15 minutes, the dissolution rate of CCCG reached $83.34 \pm 2.39\%$, while the dissolution rate of CCD was only $70.74 \pm 2.18\%$ (Figure 1(d)). This further supported the conclusion that CCCG had superior pharmaceutical advantages over CCD and promoted the release of calcium ions more effectively.

3.2. Drug Permeability of CCCG. The integrity of Caco-2 cell monolayer was evaluated with fluorescence sodium, a commonly used marker. At all timing, P_{app} of fluorescence sodium was almost the same (Figure 1(f)), which suggested a compact cell monolayer of Caco-2 was established, though it was not statistically significant.

Calcium concentration of samples collected was measured as mentioned above at each timing; P_{app} of both CCCG and CCD were quantified. As Figure 1(g) showed, P_{app} of CCCG rose over time, while CCD had an opposite potential. And at last, P_{app} of CCCG was significantly higher than CCD at 60 min ($9.98 \times 10^{-3} \pm 0.19 \times 10^{-3}$ vs $3.66 \times 10^{-3} \pm 0.18 \times 10^{-3}$ cm/s, $^*P < 0.05$), indicating that CCCG could be more absorbed in the intestinal environment.

3.3. Antiosteoporosis Effect of CCCG in Mice. After 21 days of RA treatment, serum calcium and phosphorus concentration of the model and control mice were measured. The concentration of blood calcium and phosphorus in the model group were $27.51 \pm 4.96\,\mu$mol/dL and 1.09 ± 0.17 mmol/dL, respectively, while those in the normal group were $47.59 \pm 4.97\,\mu$mol/dL and 2.07 ± 0.26 mmol/dL. Serum concentration in the model group was statistically lower than the normal group, suggesting bone formation with calcium was interfered, while calcium and phosphorus in the normal group could still precipitate in the process (Figure 2(a)). The OP model was also subjected to femoral micro-CT testing. Micro-CT 2D reconstruction results showed that the amount of the trabecular bone in the model group reduced and its density was lower than the control group (Figure 2(b)). In addition, BV/TV ($34.26 \pm 2.64\%$ vs. $26.07 \pm 2.05\%$) and Tb.Th (0.16 ± 0.01 mm vs. 0.11 ± 0.01 mm) showed significant decrease in the OP model mice, while Tb.Sp (0.36 ± 0.01 mm vs. 0.43 ± 0.01 mm) slightly increased (Figure 2(c)). As a result, osteoporosis models were successfully established.

In all drug-treated mice, regain on body weight was observed (Figure 2(d)). Diameter of the femur and total mass of the femur and tibia from the model mice increased after CCCG administration, while the difference in femur length was not significant (Figures 2(e) and 2(f)). The analysis of the organ mass index showed that CCCG could ameliorate the liver and spleen index induced by retinoic acid, but there were no significant differences compared with model groups (Figure 2(g)).

Table 3: Particle size and cumulative distribution of CCCG.

Drug	D10 (μm)	D50 (μm)	D90 (μm)	D (4,3) (μm)
CCCG	252.09 ± 15.42	904.19 ± 24.45	1930.75 ± 97.98	1026.66 ± 39.59
CCD	460.88 ± 14.58**	1429.17 ± 59.18**	2540.68 ± 121.20*	1482.42 ± 53.59**

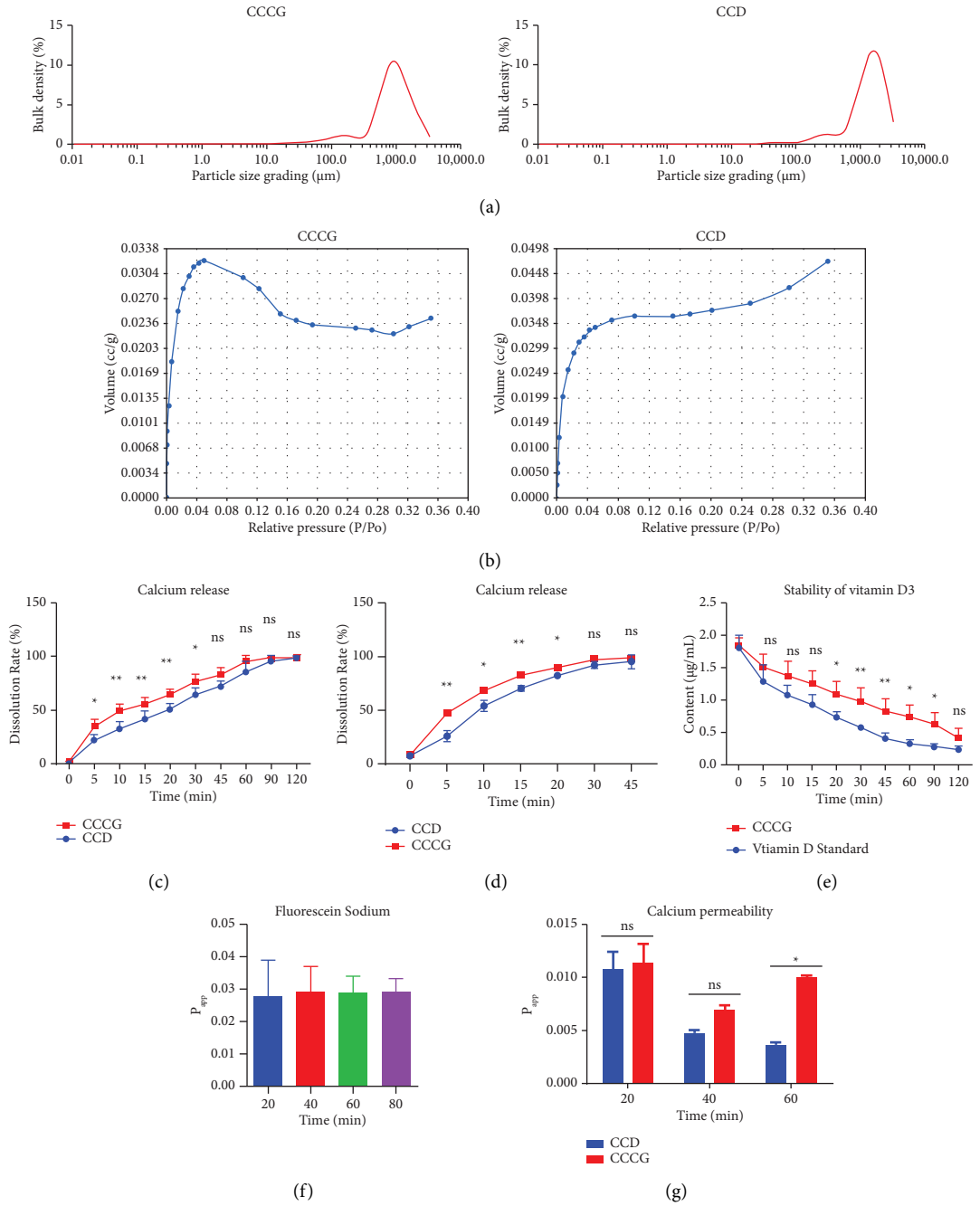

Figure 1: The pharmaceutical advantage of CCCG. (a) Particle size distribution map of CCCG and CCD. (b) BET nitrogen adsorption desorption isotherm of CCCG and CCD. Comparison of calcium ion release rates from unground (c) or grounded. (d) CCCG and CCD granules. (e) Determination of vitamin D_3 stability in vitro. Apparent permeability coefficients (P_{app}) of fluorescein sodium and calcium at different timing. (f) P_{app} of fluorescein sodium at different timing. (g) P_{app} of CCCG and CCD evaluated with calcium concentration. $^*P < 0.05$, and $^{**}P < 0.01$; $n = 3$ or 4 per group.

Table 4: BET nitrogen desorption data with different fillers.

Drug	BET-specific surface area (m^2/g)	(αs) Pore-specific surface area (m^2/g)	Mean pore radius (nm)	Pore volume (cc/g)
CCCG	0.080 ± 0.01	0.104 ± 0.002	1.12 ± 0.06	$(4.3 \pm 0.6) \times 10^{-5}$
CCD	0.103 ± 0.02	0.112 ± 0.007	1.17 ± 0.04	$(5.9 \pm 1.1) \times 10^{-5}$

Table 5: Particle size and BET-specific surface area of grinding CCCG and CCD.

Drug	D (4,3) (μm)	BET-specific surface area (m^2/g)
CCCG	105.24 ± 3.92	0.39 ± 0.03
CCD	108.30 ± 4.41	0.43 ± 0.05

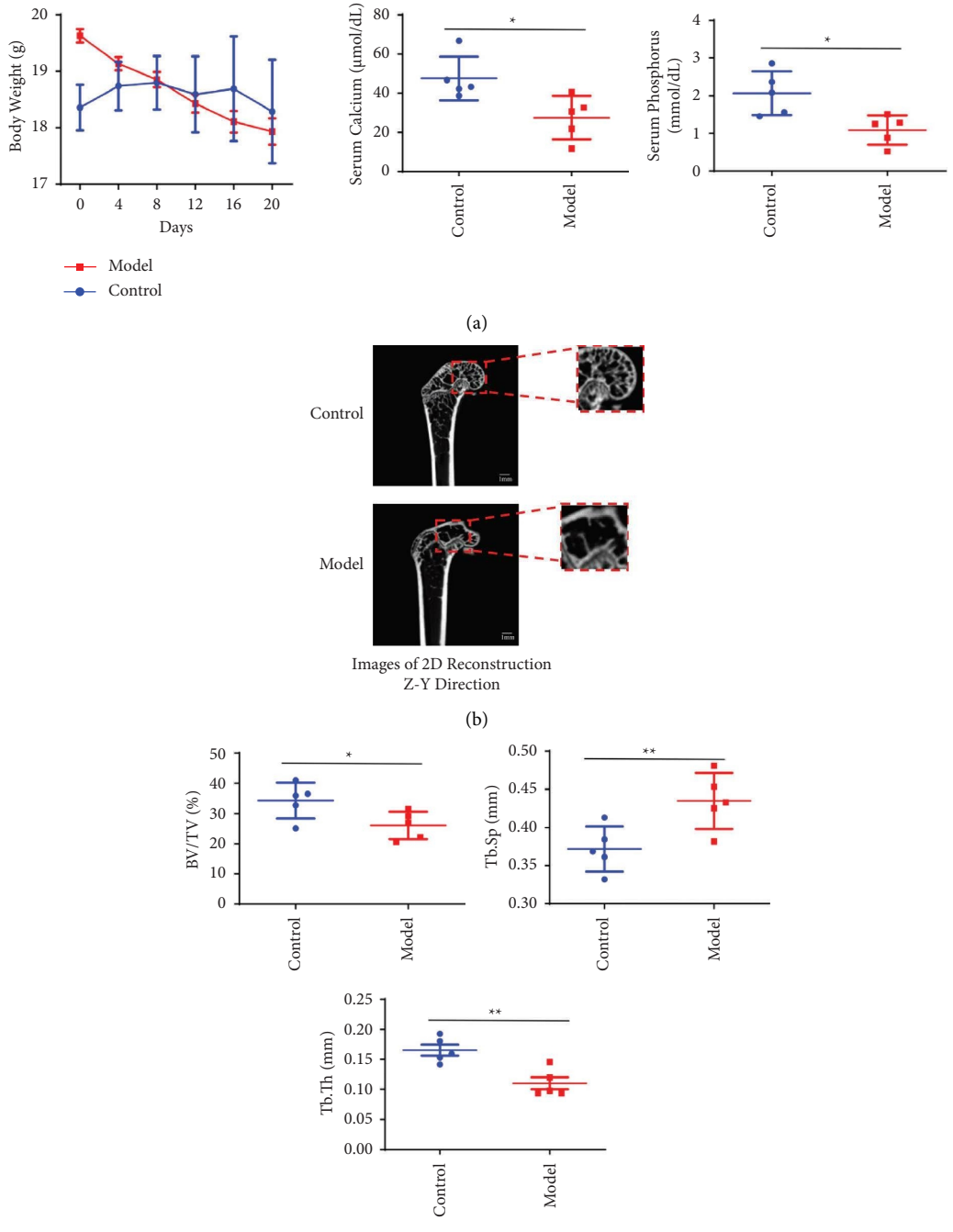

Figure 2: Continued.

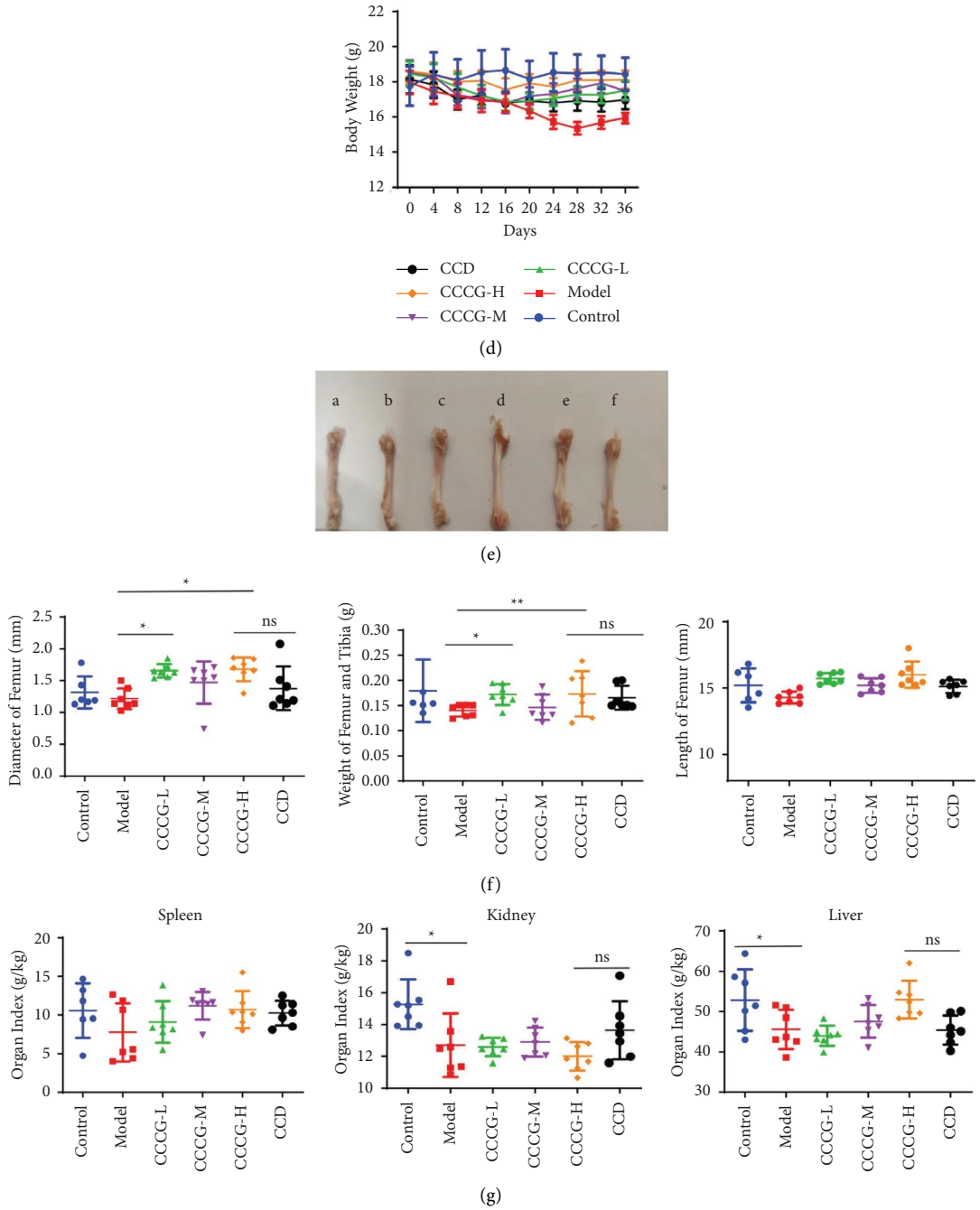

Figure 2: CCCG improved femoral and tibia deterioration, body weight, and organ index in osteoporosis (OP) mice. (a) The selected OP model was constructed using RA and subjected to test blood calcium, blood phosphorus, and body weight 21 d after gavage. (b, c) Images of 2D reconstruction obtained by micro-CT and the microstructure parameters of BV/TV, Tb.Th, and Tb.Sp was compared between the control and model groups ($n = 5$). (d) Effects of treatment with CCCG at different doses on body weight for 36 days. (e) Images of the femur of the right leg of mice in different experimental groups. A: control group; B: model group; C: CCCG-low; D: CCCG-medium; E: CCCG-high; F: CCD. (f) Length and diameter of femurs, weight of the femur and tibia. (g) Organ index of the kidney, liver, and spleen. Control: normal mice; model: RA-induced OP model mice; CCCG-L: low-dose CCCG-treated OP model mice; CCCG-L: middle-dose CCCG-treated OP model mice; CCCG-H: high-dose CCCG-treated OP model mice; CCD: CCD-treated OP mice. $^{*}P < 0.05$, and $^{**}P < 0.01$; $n = 6$ or 7 per group.

3.4. Effects of CCCG on Bone Metabolism and Oxidation Stress in OP Mice. In model mice, serum calcium, phosphorus, BALP, PINP, and OPG levels were statistically lower than normal mice ($^{*}P < 0.05$; Figures 3(a)–3(e)). All CCCG-treated mice had higher measures than model mice ($^{*}P < 0.05$), but no significant difference was observed in the OPG level of CCCG-high dose (CCCG-H) mice (Figure 3(e)). Concentration of BALP and calcium in serum

of mice in the CCCG-H group was 7.45 ± 0.31 ng/mL and 38.74 ± 2.76 μmol/dL, respectively. While the concentration of those in serum of mice in the CCD group was 5.55 ± 0.24 ng/mL and 26.89 ± 3.27 μmol/dL, suggesting that CCCG was superior to CCD in improving bone metabolism of OP mice. The median effective dose (ED_{50}) of CCCG to improve BALP was 1.13 g/kg. All calcium-treated mice showed an increase in such indicators. In the kidney, the MDA level was higher, but no significant difference was observed in CAT and SOD levels (Figure 3(f)); in the liver, osteoporosis model mice had higher MDA and lower CAT and SOD levels (Figure 3(g)). These results indicated that CCCG might have a potent effect on affiliating the intrinsic antioxidant system.

3.5. Effects of CCCG on Bone Microstructures and Bone Growth. The trabecular microstructure of the femur was characterized by micro-CT after the administration of CCCG or CCD. 2D and reconstructed 3D images provided a picturesque view of bone trabeculae from the far side of mice femurs treated differently (Figure 4(a)). We could explicitly find a decrease in bone quantity and an increase in the pore rate in the model group. In CCCG medium and high-dose groups, higher bone mass density and lower pore rate could be observed.

ROI was analysed according to quantified micro-CT results of the femur far side. Model mice exhibited lower BV/TV, Tb.N, and Tb.Th than normal mice, but significantly higher Tb.Sp and Tb.Pf (Figures 4(b)–4(f)). These results suggested that RA brought up a descend on the bone mass density on mouse femurs. As a result of CCCG treatment, the increase in Tb.Sp and Tb.Pf was lower in CCCG mice than models; the decrease in BT/TV, Tb.Th, and Tb.N was also recovered. The ED_{50} of CCCG for increasing the proportion of BV/TV was 1.15 g/kg calculated by prism 6.0. CCCG medium or high dose-treated mice were found to have significant restoration on observed parameters including Tb.Th and Tb.Pf (Figures 4(c) and 4(f)). Femurs were evaluated via a three-point bending test to determine the biomechanical status of the cortical bone. The results showed that the maximum load and deflection, fracture energy, and stiffness were significantly lower in the model group than those in the control group (Figures 4(g)–4(J)), and increased in both middle- and high-CCCG groups when compared with the model group ($P < 0.01$). In addition, stiffness was significantly higher in the CCCG-H group than in the model group ($P < 0.01$). The therapeutic outcome of CCCG-H was also more satisfying than that of CCD.

To investigate the effect of CCCG on the number of femoral trabecular cells, H&E staining was used to observe pathological changes in the distal femurs and trabecular bones. Compared to control mice, less bone trabeculae were observed in model mice; trabeculae were found thinner and had an apparent lower density, which went in accordance with results of micro-CT detection. Loss of bone marrow could be observed, and cartilage fibrosis was also found in model mice (Figure 4(k)). In CCCG low dose (CCCG-L), medium dose (CCCG-M), and CCD-treated bones, the trabecular bone became abundant. Especially, newly formed bones were found in CCCG-L mice. In CCCG-H bones, no injuries were found in the bone structure, bone trabeculae presented slight loss together with the compact texture.

3.6. Effects of CCCG on Osteogenic Differentiation of HOS. According to the determination of cell viability, the half maximal inhibitory concentration (IC_{50}) value of CCCG cannot be calculated. When the concentration of CCCG was 1 mg/mL, the inhibition rate was $7.29 \pm 3.82\%$ (Figure 5(a)). Cell viability of HOS reached the peak when 200 μg/mL CCCG was administered (Figure 5(a)). ALP staining and mineralized nodules staining showed a positive correlation on CCCG concentration (Figures 5(b) and 5(c)). Similar observations were found in ALP activity and mineralized nodules quantitative analysis of whole-well in HOS cells (Figures 5(b) and 5(c)).

The effect of CCCG on the expression of genes related to osteogenic functions was detected after 48 h of treatment. A significant upregulation was detected in osteoblast differentiation-related genes like bone morphogenetic protein 2 (BMP2), RUNX2, ALP, and osteopontin (OPN) (Figure 5(e)). Western blotting showed that RUNX2 and β-catenin levels increased as the concentration of CCCG increased (Figure 5(d)). This could be the proof that CCCG could accelerate the restoration of osteoporosis fractures.

3.7. CCCG Reduced Urine Calcium Concentration and Increased Urine pH in OP Mice. Usually, after a long-term administration of calcium carbonate, the concentration of calcium and the acidity of urine would increase, which could promote the formation of stones, and make calcium urate and calcium oxalate easier to precipitate. With the increase of CCCG dose, urine pH grew. Among the results, the average pH of urine from CCCG-H mice was 6.86 ± 0.21, while the model group was 5.82 ± 0.21 with a significant difference, indicating that CCCG significantly reduced the acidity of urine of OP mice. (Figure 6(a)). When pH was higher than 6.5, urinary acid tended to be unsaturated and not to participate in precipitation, meanwhile previous stones would also dissolve. Calcium concentration was measured by the SpectrAA-240FS FAAS system. A decrease of urine calcium concentration in CCCG-H could be found in comparison to CCD-treated mice. The concentration of urine calcium ions of CCCG-H mice was 2.27 ± 0.48 mg/L, and that of CCD mice was 5.48 ± 0.87 mg/L, which could be the sign of lower risk of kidney stone caused by CCCG (Figure 6(b)).

4. Discussion

Calcium carbonate is widely used to supplement calcium, primarily because of its high calcium load and low cost [9]. The combination of calcium with vitamin D_3 forms the basis of preventive and therapeutic regimens for osteoporosis. Studies have shown that the capacity of the small intestine to absorb calcium salts depends on the solubility and ionization of the salt. Fasting calcium citrate absorption is greater than that of calcium lactate and calcium carbonate [15]. The

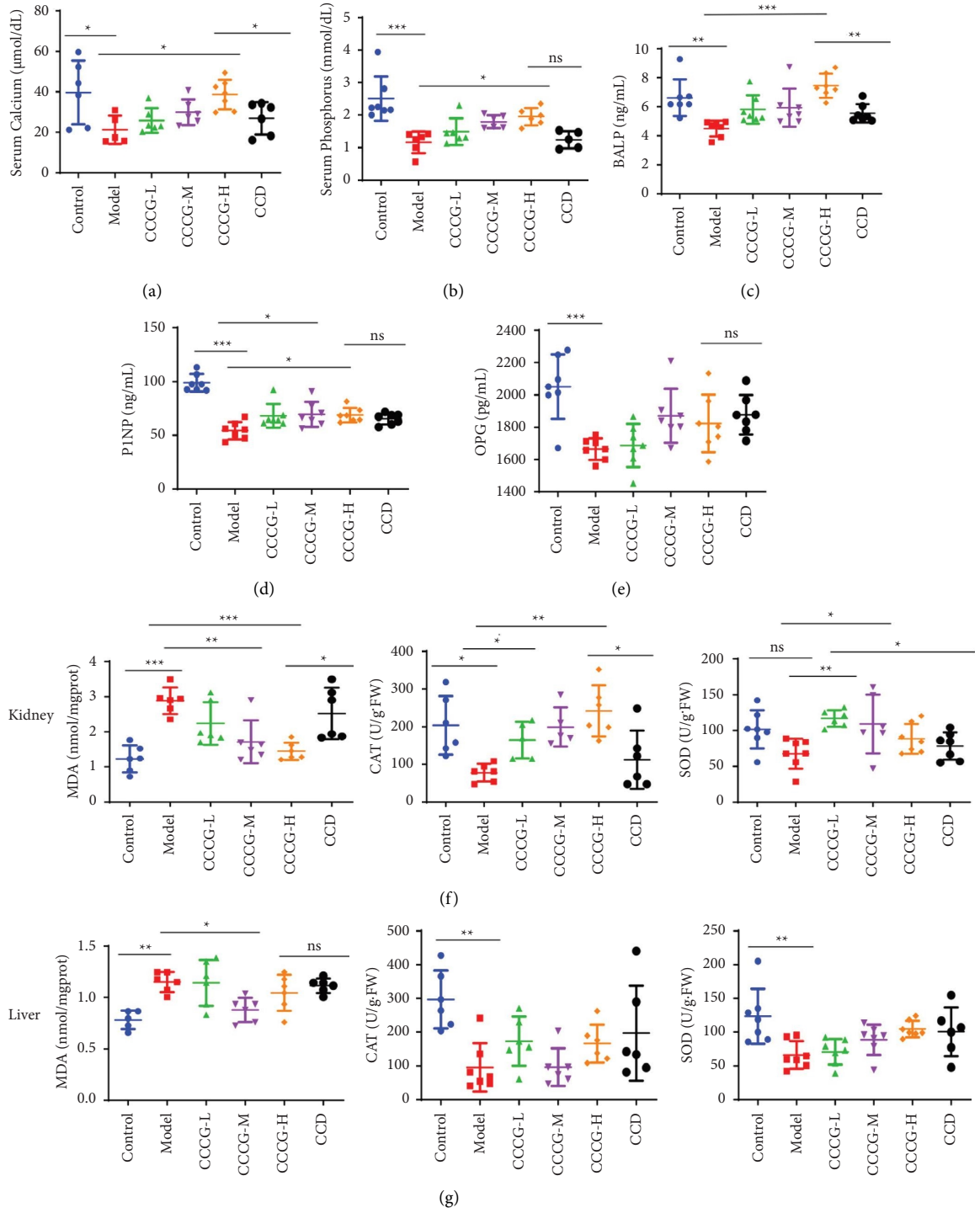

Figure 3: CCCG improved bone metabolism in osteoporosis (OP) mice. Laboratory tests for biochemical markers of bone metabolism: serum bone metabolism-related indicators calcium (a), phosphorus (b), BALP (c), P1NP (d), and OPG (e) were determined after the administration of CCCG or CCD for 36 days; (f, g) oxidative stress-related kidney and liver superoxide dismutase (SOD), malondialdehyde (MDA), and catalase (CAT) were determined after the administration of CCCG or CCD. Control: normal mice; model: RA-induced OP model mice; CCCG-L: low-dose CCCG-treated OP model mice; CCCG-M: middle-dose CCCG-treated OP model mice; CCCG-H: high-dose CCCG-treated OP model mice; CCD: CCD-treated OP mice. $^{*}P < 0.05$, $^{**}P < 0.01$, and $^{***}P < 0.001$; $n = 6$ or 7 per group.

limitation of the calcium carbonate supplements currently used includes the adverse effects on gastrointestinal tract and urinary calculus. They are manifested by the change of gastric emptying, the increase of calcium ion concentration in urine and urine acidity, which can promote the formation of calculus [20, 21]. In addition to calcium supplement, it is worth noting that calcium carbonate exists in various polymorphs, such as calcite, aragonite, and vaterite [22].

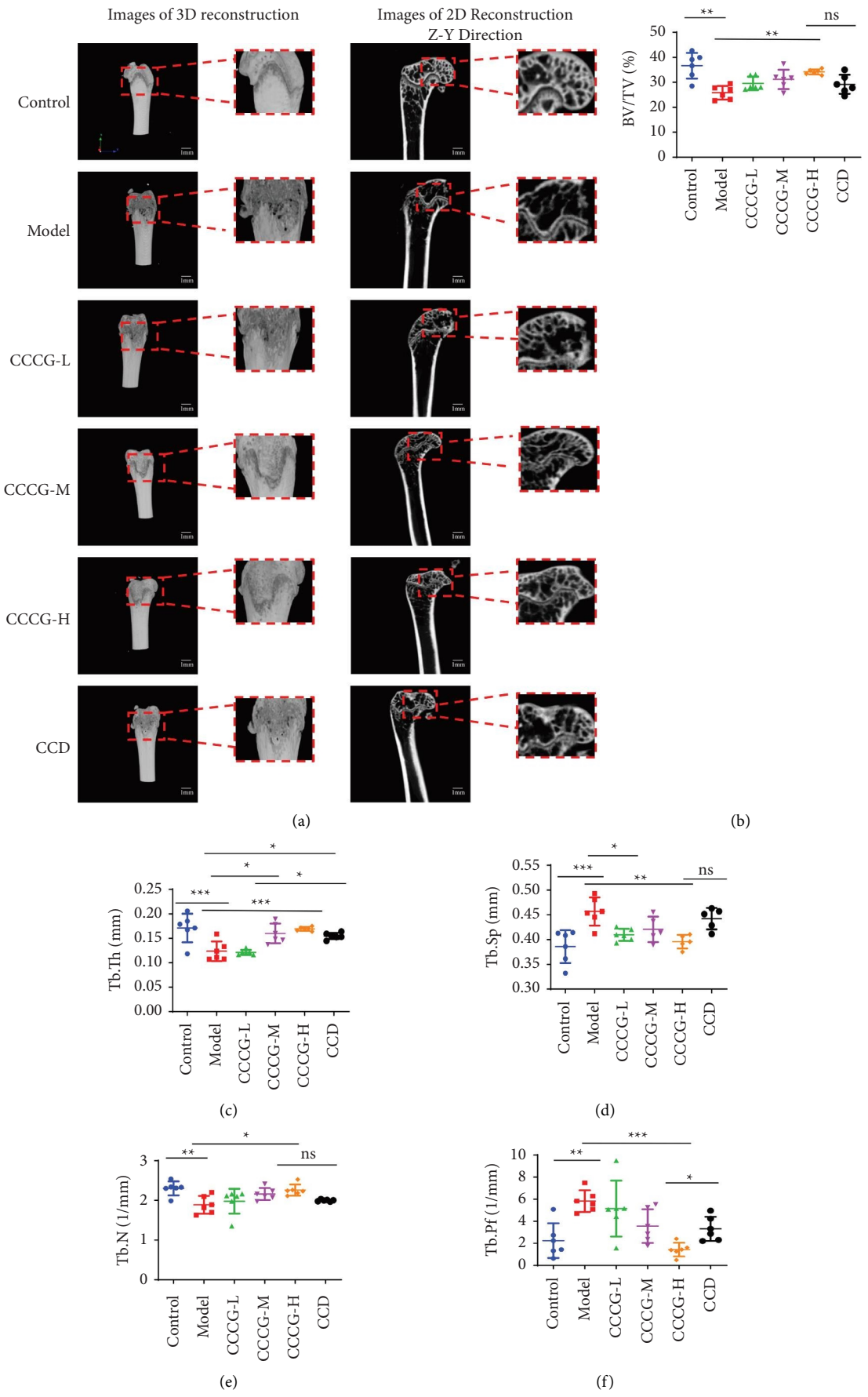

Figure 4: Continued.

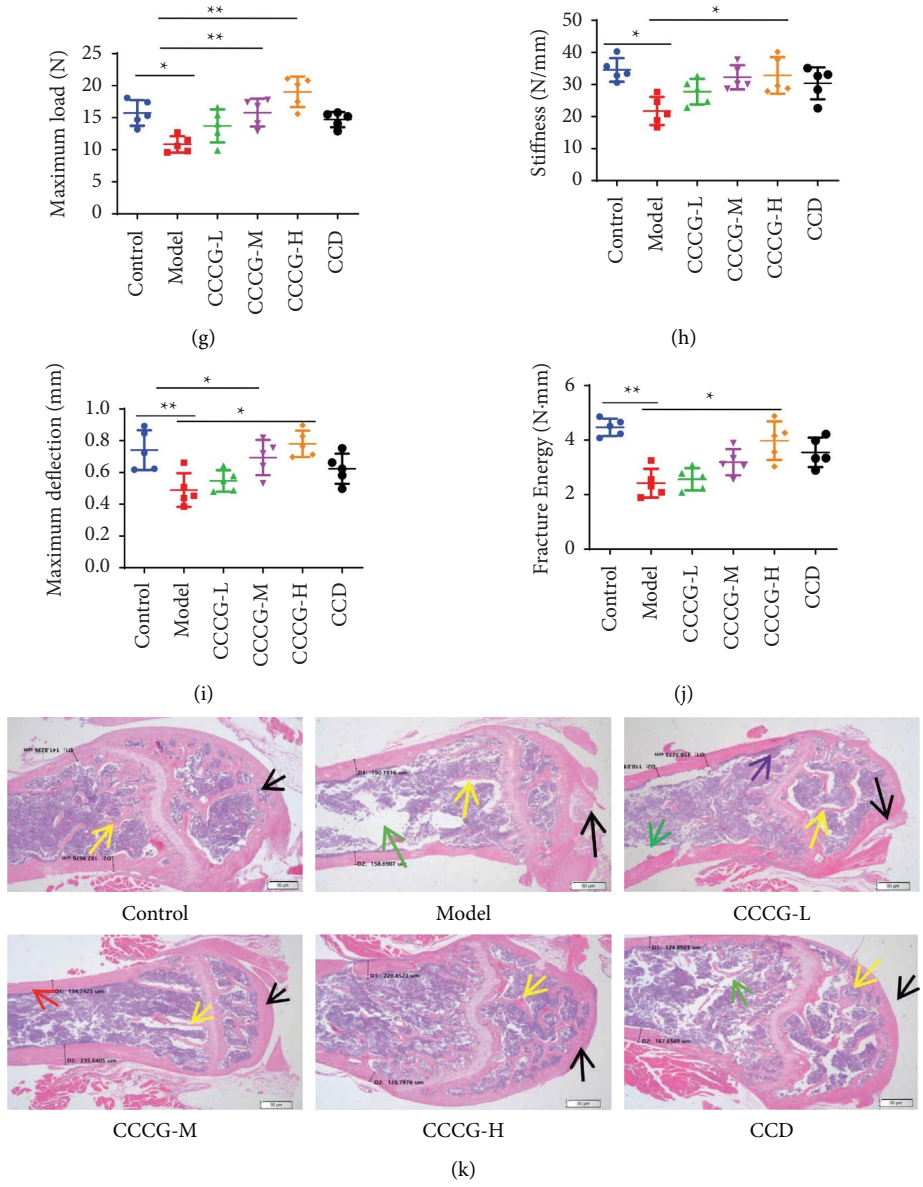

Figure 4: Effects of CCCG on the femur microstructure and bone growth of osteoporosis (OP) model mice: (a) images of 2D and 3D reconstruction obtained by micro-CT after the administration of CCCG or CCD. The red arrow represented the *X*-axis, the blue arrow showed the *Y*-axis, and the green arrow indicated the *Z*-axis. Microstructure parameters of BV/TV (b), Tb.Th (c), Tb.Sp (d), Tb.N (e), and Tb.Pf (f) were detected. (g–j) Changes in the biomechanical characteristics of the femur, including maximum load, stiffness, maximum reflection, and frame energy. (k) 36 days after CCCG or CCD administration, H&E staining (40X) was used to observe the pathological changes of the distal femur. Yellow arrows indicated trabeculae; black arrows represented cartilage; green arrows represented bone marrow cavity; purple arrows showed a small amount of new bone, and red arrows represented the cortical bone. Control: normal mice; model: RA-induced OP model mice; CCCG-L: low-dose CCCG-treated OP model mice; CCCG-M: middle-dose CCCG-treated OP model mice; CCCG-H: high-dose CCCG-treated OP model mice; CCD: CCD-treated OP mice. $^{*}P < 0.05$, $^{**}P < 0.01$, and $^{***}P < 0.001$; $n = 6$ per group.

Among these polymorphs, vaterite has gained attention for its potential biomedical applications, particularly in promoting bone formation, supporting blood vessel formation, and facilitating bone defect repair [23]. In this study, calcium carbonate was converted to a water-soluble calcium citrate complex via complexation techniques, independent of gastric acid, which might help to prevent abdominal distension and flatulence, as well as minimized the risk of renal calculus formation. Therefore, we proved that the CCCG, a novel calcium carbonate composite particles had obvious pharmaceutical and pharmacodynamic advantages over (CCD).

The past decades have witnessed the emergence of multiple pharmacological agents for osteoporosis of more targeting capability or effectiveness, but calcium doses supplemented with vitamin D is still a widely considered choice due to lower costs [24]. However, poor absorption rate of calcium and the adverse effect of kidney stone are

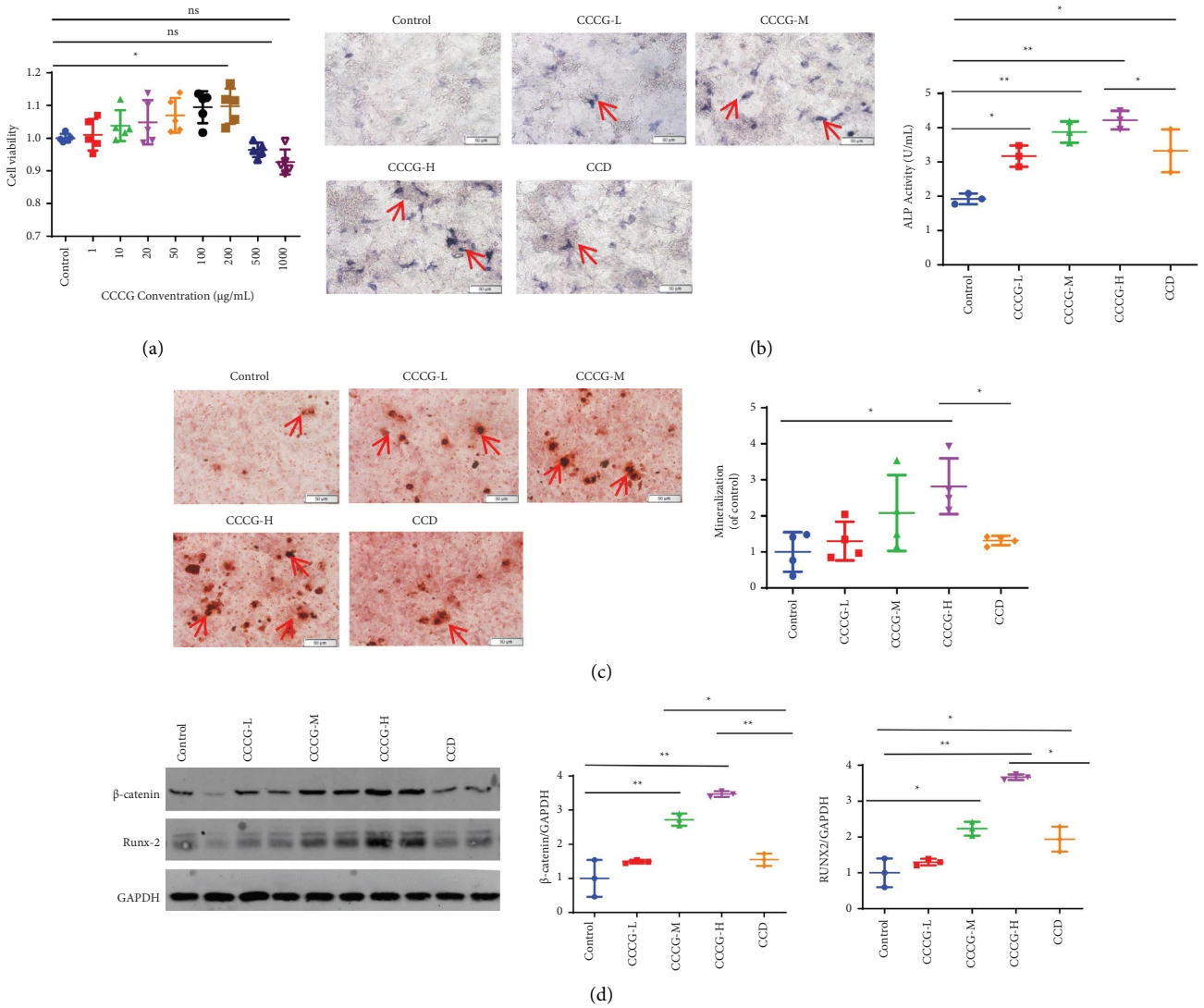

Figure 5: Continued.

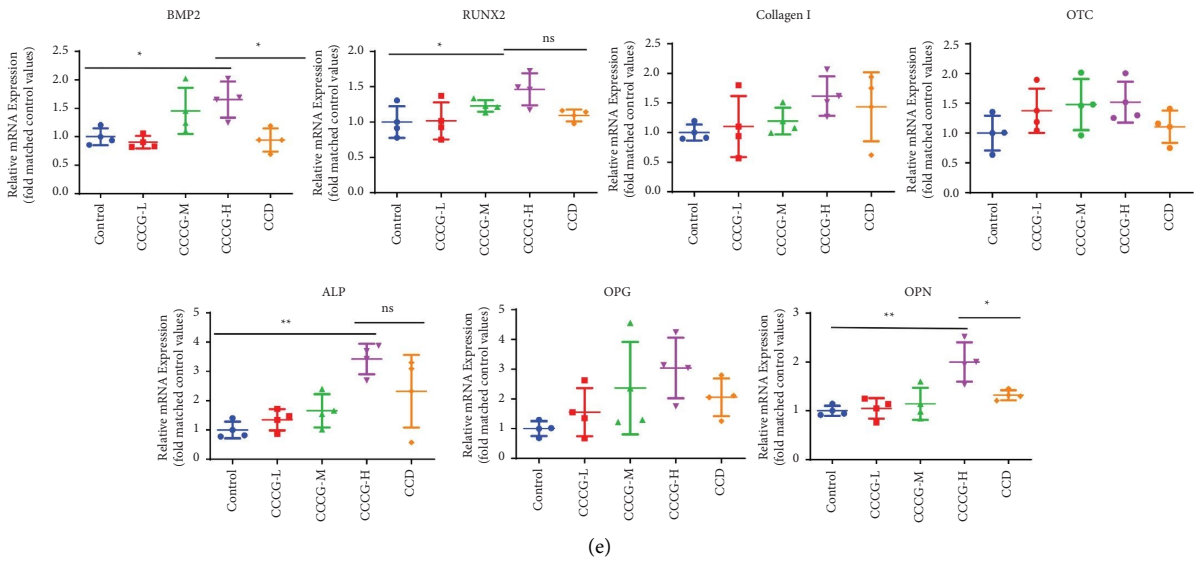

Figure 5: CCCG promoted osteogenic differentiation of HOS cell in vitro: (a) the effect of CCCG on HOS cells activity was determined by CCK-8 compared to control groups ($n = 5$). (b) ALP staining and activity quantitative in HOS cells after drug administration ($n = 3$). Under the catalysis of alkaline phosphatase, BCIP is hydrolyzed to produce a highly reactive product, which reacted with NBT to form an insoluble dark blue to blue-purple NBT-Formazan. The red arrow indirectly represented the enzyme activity of ALP. (c) Mineralized nodule staining and quantitative analysis of mineralized nodules in HOS cells. Red arrows represented calcium nodules (orange-red deposits). (d) Representative western blots showing β-catenin and Runx-2 protein expression of HOS cells, treated with or without CCCG for 48 h ($n = 3$). (e) RT-qPCR was used to quantify the mRNA expression of osteogenic marker genes ALP, RUNX2, COL-I, OTC, OPN, BMP2, and OPG, treated with or without CCCG for 48 h. The mRNA expression levels were normalized to the mRNA expression of GAPDH ($n = 4$). Control: HOS cells were cultured in osteogenic induction medium; CCCG-L: HOS cells were cultured in osteogenic induction medium with low-dose CCCG; CCCG-M: HOS cells were cultured in osteogenic induction medium with middle-dose CCCG; CCCG-H: HOS cells were cultured in osteogenic induction medium with high-dose CCCG; CCD: HOS cells were cultured in osteogenic induction medium with CCD. $^{*}P < 0.05$, and $^{**}P < 0.01$.

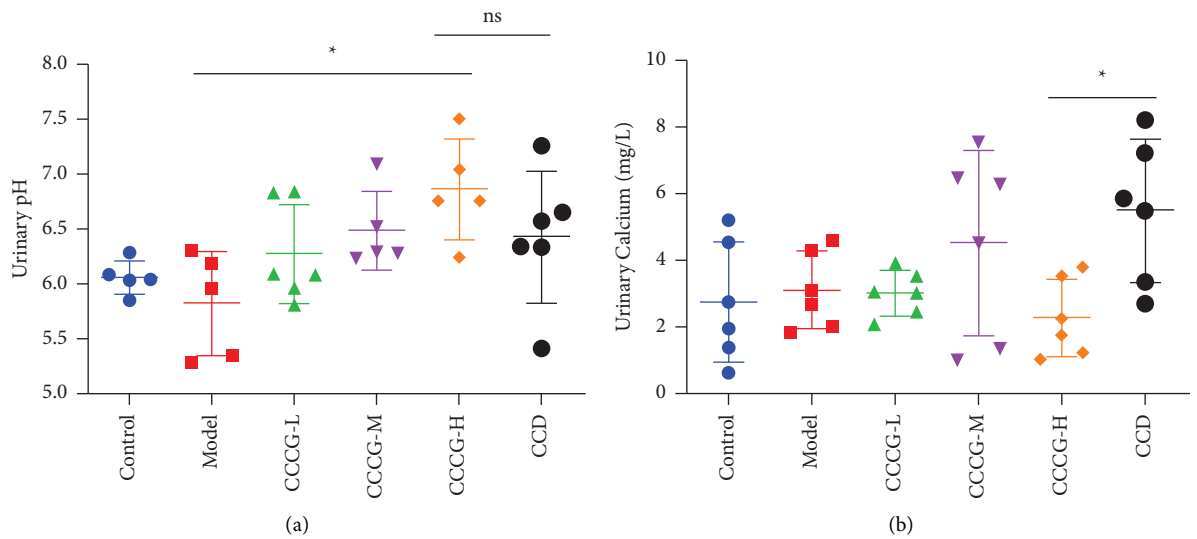

Figure 6: CCCG reduced the possibility of urolithiasis: effects of CCCG on urine pH (a) and calcium concentration (b) in mice. Control: normal mice, model: retinoic acid (RA)-induced OP model mice; CCCG-L: low-dose CCCG-treated OP model mice; CCCG-M: middle-dose CCCG-treated OP model mice; CCCG-H: high-dose CCCG-treated OP model mice; CCD: CCD-treated OP mice. $^{*}P < 0.05$; $n = 5$ or 6 per group.

always annoying problems for most of the calcium supplements in the market [25]. In this study, we were trying to prove that CCCG could be a better choice for daily calcium supplement with the unique pharmaceutical properties.

The dissolution rate has been one of the main drawbacks of calcium supplements; the stability of vitamin D_3 also plays a role in the evaluation of efficacy. In our study, CCCG exhibited higher dissolution rate, and a smoother degradation curve of vitamin D_3 was observed, which indicated a preferable stability. Transepithelial permeability of CCCG was evaluated using a cell monolayer model of Caco-2, where CCCG displayed a better absorption profile. In short, CCCG showed superior pharmaceutical profiles than CCD.

The release rate of calcium ions and the stability of vitamin D_3 depend on the size of granules, surface area and material reactivity. CCCG showed superior pharmaceutical advantages over CCD in terms of particle size. Spray-drying was utilized to achieve smaller and more uniform particles for CCCG. The BET-specific surface area between CCCG and CCD was not significantly different. Particles with higher material reactivity dissolve faster due to increased chemical reactivity. Compared to CCD, CCCG had a faster dissolution rate. This might be attributed to the use of sodium bicarbonate as a catalyst in its formulation, which accelerated the chelation reaction and balanced the pH of the solution around 6. This, in turn, increased its chemical reactivity. The above mentioned results demonstrated that CCCG's advantages of small particle size and material reactivity lead to a good calcium ion release rate. Further grinding was conducted on CCCG and CCD granules to reach uniform particle size and surface area. The results showed that the release of calcium ions of CCCG was higher than that of CCD at 5–20 min, further embodying the advantages of CCCG's material reactivity. Vitamin D_3 in CCCG was a β-cyclodextrin inclusion complex of vitamin D_3, which significantly improved the stability and content of vitamin D_3. $_3$. Taken together, from the positive effects of these factors, we can gain a more comprehensive understanding of the pharmaceutical advantages of CCCG.

In recent years, RA-induced OP model has been widely used in the study of drug-induced secondary OP [19]. Compared with the long and complex experimental process of ovariectomized (OVX) model, the RA-induced osteoporosis model is more simple, rapid, and highly successful and presents typical symptoms of osteoporosis. At the same time, it has been reported that RA can damage ovarian function, reduce estrogen levels, and affect the occurrence of osteoporosis [26].

We explored variation in bone trabeculae, bone metabolic markers, as well as liver and kidney oxidative stress between differently treated mice. PINP and BALP are the indicators of osteogenesis [27–29]; OPG, also named osteoclastogenesis inhibitory factor (OCIF), inhibits osteoclastogenesis and bone resorption through receptor activator of nuclear factor-kappa B (RANK)/RANKL/OPG axis [30]. In vivo assays, mice treated with CCCG were observed to have higher reads in such markers, which indicated the capability of CCCG to promote osteogenesis and therefore attenuate osteoporosis. Histological analysis, biomechanical parameter analysis, and micro-CT imaging on bones provided a more explicit sight into tissues and microstructures of bones. And our results supported the therapeutic effect of CCCG on osteoporosis, reversing the pathogenetic process. Oxidation stress can promote osteoporosis by inhibiting osteoblast differentiation [30–32]; SOD and CAT are essential antioxidant enzymes, while MDA is the oxidant metabolite of lipid [34, 35]. Our assays showed that CCCG played a role in the promotion of the intrinsic antioxidant system, attenuating its damage on osteogenesis. HOS could be used to evaluate osteogenic differentiation. Assays on the cell model showed that CCCG raised the viability of osteoporosis-related cells, accompanied with accelerated bone recovery.

Urine calcium concentration has a strong link with bone formation and calcium resorption [36, 37]. CCCG exhibited a low urine calcium concentration and high pH. Higher pH can provide an environment where oxalate and phosphorus tend to remain their molecular form, and therefore reducing the risk of kidney stone. On the other hand, higher pH can increase the stability of vitamin D_3 [38], and in our preliminary observation, higher pH could also reduce the dependence on gastric acid to digest calcium carbonate. And taken together, these findings indicated that CCCG facilitated calcium absorption in gastrin, together with lower possibility of nephrolithiasis.

According to the preparation of CCCG, the chemical composition of CCCG showed that they contain hydroxyl groups and carbonates which were similar to the chemical composition of the bone. Furthermore, calcium citrate, which was the affecting element in our formulation, had been shown to have a better bioavailability than calcium carbonate due to its higher solubility and ionization in the gastrointestinal tract. The improved absorption of calcium could lead to better bone mineral density and potentially reduce the risk of osteoporosis. In addition, our formulation had a higher pH, which could create an environment that was more conducive to bone formation and mineralization. Overall, CCCG's material properties matched that of the bone in respect with chemistry.

While bone tissues and properties differ between mice and humans, animal models remain an important tool for preclinical tests of drugs before human trials. In our study, the RA-induced osteoporosis mice model may not fully replicate the pathophysiology of osteoporosis in humans, but this model has been widely used in the drug-induced secondary osteoporosis and is able to present typical symptoms of osteoporosis. The Caco-2 cell monolayer model provides a simplified representation of the human small intestine. Nonetheless, this model has been extensively used to study intestinal absorption of nutrients and drugs and can provide valuable information for further research. At present, CCCG has been granted a patent number 201110139889.8, clarifying that CCCG has entered the clinical stage and achieved drug conversion, which provides a certain degree of guarantee for its safety and effectiveness in the human body.

Overall, this study provided a relatively comprehensive insight on this intriguing calcium formulation from both its efficacy and pharmaceutic profiles. First, the pharmacological advantage of CCCG against osteoporosis was illustrated using multiple approaches, and from here, we could explain its pharmaceutic advantages in calcium ion release and vitamin D_3 stability and better drug absorption compared to general calcium carbonate granules; other than that, there was also a lower morbidity of kidney stone.

5. Conclusions

The novel calcium formulation described here may be therapeutically advantageous over commonly used calcium carbonate granules because of its superior stability, dissolution rate, and permeability characteristic. On the other hand, CCCG was proved to have a preferable anticipation on the outcome of osteoporosis. And the complexation technology was used to convert calcium carbonate into water-soluble calcium citrate complex, which minimized the risk of kidney stone formation. To sum up, CCCG can be more safe and effective to prevent and treat osteoporosis, fracture healing, osteopenia, rickets, and other diseases caused by calcium deficiency.

Abbreviations

CCCG: Compound calcium carbonate granule
CCD: Calcium carbonate with vitamin D
RA: Retinoic acid
BMD: Bone mineral density
NIH: National Institute of Health
IOM: Institute of Medicine
FAAS: Flame atomic absorption spectroscopy
P_{app}: Apparent permeability factor
BALP: Bone alkaline phosphatase
PINP: Propeptide type I N-terminal precollagen
OPG: Osteoprotegerin
MDA: Malondialdehyde
SOD: Superoxide dismutase
CAT: Catalase
BV/TV: Trabecular bone volume
Tb.Th: Trabecular thickness
Tb.Sp: Trabecular separation
Tb.N: Trabecular number
Tb.Pf: Trabecular pattern factor
ALP: Alkaline phosphatase
ROI: Regions of interest
RUNX2: Runt-related transcription factor 2
OP: Osteoporosis
ANOVA: Analysis of variance
COL-I: Collagenase I
OTC: Ornithine transcarbamylase
OPN: Osteopontin
BMP2: Bone morphogenetic protein 2.

Data Availability

The data used to support the findings of this study are included within the article or supplementary materials.

Ethical Approval

The animal study protocol was approved by the Animal Care and Use Committee of Huazhong University of Science and Technology (IACUC; number: 2671).

Conflicts of Interest

The authors declare that they have no conflicts of interest.

Authors' Contributions

MK deigned the study, conducted the experiments, and analysed the data. HJL wrote the manuscript. YHM, HJY, and HJL contributed to conduct experiments and data collection. XM supervised the whole project and revised the manuscript. All authors have read and approved the final version of the manuscript.

Supplementary Materials

Figures S1: Original Western blotting results of HOS cell treated with CCCG and CCD. (*Supplementary Materials*)

References

[1] J. P. van den Bergh, P. Szulc, A. M. Cheung, M. Bouxsein, K. Engelke, and R. Chapurlat, "The clinical application of high-resolution peripheral computed tomography (HR-pQCT) in adults: state of the art and future directions," *Osteoporosis International*, vol. 32, no. 8, pp. 1465–1485, 2021.

[2] Q. Zeng, N. Li, Q. Wang et al., "The prevalence of osteoporosis in China, a nationwide, multicenter DXA survey," *Journal of Bone and Mineral Research*, vol. 34, no. 10, pp. 1789–1797, 2019.

[3] J. E. Compston, M. R. McClung, and W. D. Leslie, "Osteoporosis," *The Lancet*, vol. 393, no. 10169, pp. 364–376, 2019.

[4] J. G. Zhao, X. T. Zeng, J. Wang, and L. Liu, "Association between calcium or vitamin D supplementation and fracture incidence in community-dwelling older adults: a systematic review and meta-analysis," *JAMA*, vol. 318, no. 24, pp. 2466–2482, 2017.

[5] M. J. Berridge, M. D. Bootman, and H. L. Roderick, "Calcium signalling: dynamics, homeostasis and remodelling," *Nature Reviews Molecular Cell Biology*, vol. 4, no. 7, pp. 517–529, 2003.

[6] NIH Consensus Development Panel on Osteoporosis Prevention, "Diagnosis, and Therapy, March 7-29, 2000: highlights of the conference," *Southern Medical Journal*, vol. 94, no. 6, pp. 569–573, 2001.

[7] F. Huang, Z. Wang, J. Zhang et al., "Dietary calcium intake and food sources among Chinese adults in CNTCS," *PLoS One*, vol. 13, no. 10, Article ID e0205045, 2018.

[8] K. E. Ensrud and C. J. Crandall, "Osteoporosis," *Annals of Internal Medicine*, vol. 167, no. 3, pp. ITC17–ITC32, 2017.

[9] H. Fausett, C. Gayser, and A. K. Dash, "Evaluation of quick disintegrating calcium carbonate tablets," *AAPS PharmSciTech*, vol. 1, no. 3, pp. 37–43, 2000.

[10] E. Letavernier and M. Daudon, "Vitamin D, hypercalciuria and kidney stones," *Nutrients*, vol. 10, no. 3, p. 366, 2018.

[11] I. P. Heilberg and D. S. Goldfarb, "Optimum nutrition for kidney stone disease," *Advances in Chronic Kidney Disease*, vol. 20, no. 2, pp. 165–174, 2013.

[12] S. Kopic and J. P. Geibel, "Gastric acid, calcium absorption, and their impact on bone health," *Physiological Reviews*, vol. 93, no. 1, pp. 189–268, 2013.

[13] Y. J. Choi, N. Kim, J. Y. Lee et al., "PMK-S005 alleviates age-related gastric acid secretion, inflammation, and oxidative status in the rat stomach," *Gut and Liver*, vol. 10, no. 5, pp. 749–756, 2016.

[14] H. D. Chen, Y. P. Chen, R. Xie, Q. Y. Hu, Q. Cheng, and M. Xiang, "Absorption characteristics of novel compound calcium carbonate granules: effects of gastric acid deficiency and exogenous weak acids," *Curr Med Sci*, vol. 39, no. 2, pp. 337–342, 2019.

[15] R. N. Johnson, "A study of five calcium supplements: estimation of calcium absorption and sodium content," *European Journal of Clinical Nutrition*, vol. 45, no. 2, pp. 117–119, 1991.

[16] M. Behbahani, P. Ghareh Hassanlou, M. M. Amini et al., "Application of solvent-assisted dispersive solid phase extraction as a new, fast, simple and reliable preconcentration and trace detection of lead and cadmium ions in fruit and water samples," *Food Chemistry*, vol. 187, pp. 82–88, 2015.

[17] J. Rakmai, B. Cheirsilp, J. C. Mejuto, A. Torrado-Agrasar, and J. J. F. H. Simal-Gándara, "Physico-chemical characterization and evaluation of bio-efficacies of black pepper essential oil encapsulated in hydroxypropyl-beta-cyclodextrin," *Food Hydrocolloids*, vol. 65, pp. 157–164, 2017.

[18] J. Yang, N. Wu, J. Peng et al., "Prevention of retinoic acid-induced osteoporosis in mice by isoflavone-enriched soy protein," *Journal of the Science of Food and Agriculture*, vol. 96, no. 1, pp. 331–338, 2016.

[19] F. Yang, J. Li, J. Zhu, D. Wang, S. Chen, and X. Bai, "Hydroxysafflor yellow A inhibits angiogenesis of hepatocellular carcinoma via blocking ERK/MAPK and NF-κB signaling pathway in H22 tumor-bearing mice," *European Journal of Pharmacology*, vol. 754, pp. 105–114, 2015.

[20] I. R. Reid, S. M. Bristow, and M. J. Bolland, "Calcium supplements: benefits and risks," *Journal of Internal Medicine*, vol. 278, no. 4, pp. 354–368, 2015.

[21] I. R. Reid, B. Mason, A. Horne et al., "Randomized controlled trial of calcium in healthy older women," *The American Journal of Medicine*, vol. 119, no. 9, pp. 777–785, 2006.

[22] M. M. Al Omari, I. S. Rashid, N. A. Qinna, A. M. Jaber, and A. A. Badwan, "Calcium carbonate," *Profiles of Drug Substances, Excipients and Related Methodology*, vol. 41, pp. 31–132, 2016.

[23] M. S. Saveleva, A. N. Ivanov, J. A. Chibrikova et al., "Osteogenic capability of vaterite-coated nonwoven polycaprolactone scaffolds for in vivo bone tissue regeneration," *Macromolecular Bioscience*, vol. 21, no. 12, Article ID e2100266, 2021.

[24] D. A. Straub, "Calcium supplementation in clinical practice: a review of forms, doses, and indications," *Nutrition in Clinical Practice*, vol. 22, no. 3, pp. 286–296, 2007.

[25] M. Wiria, H. M. Tran, P. H. B. Nguyen, O. Valencia, S. Dutta, and E. Pouteau, "Relative bioavailability and pharmacokinetic comparison of calcium glucoheptonate with calcium carbonate," *Pharmacol Res Perspect*, vol. 8, no. 2, Article ID e00589, 2020.

[26] S. Zhao, F. Niu, C. Y. Xu et al., "Diosgenin prevents bone loss on retinoic acid-induced osteoporosis in rats," *Irish Journal of Medical Science*, vol. 185, no. 3, pp. 581–587, 2016.

[27] P. Magnusson, C. A. Sharp, and J. R. Farley, "Different distributions of human bone alkaline phosphatase isoforms in serum and bone tissue extracts," *Clinica Chimica Acta*, vol. 325, no. 1-2, pp. 59–70, 2002.

[28] L. P. Seguro, C. B. Casella, V. F. Caparbo et al., "Lower P1NP serum levels: a predictive marker of bone loss after 1 year follow-up in premenopausal systemic lupus erythematosus patients," *Osteoporosis International*, vol. 26, no. 2, pp. 459–467, 2015.

[29] J. P. van Straalen, E. Sanders, M. F. Prummel, and G. T. Sanders, "Bone-alkaline phosphatase as indicator of bone formation," *Clinica Chimica Acta*, vol. 201, no. 1-2, pp. 27–33, 1991.

[30] B. F. Boyce and L. Xing, "Functions of RANKL/RANK/OPG in bone modeling and remodeling," *Archives of Biochemistry and Biophysics*, vol. 473, no. 2, pp. 139–146, 2008.

[31] N. Mody, F. Parhami, T. A. Sarafian, and L. L. Demer, "Oxidative stress modulates osteoblastic differentiation of vascular and bone cells," *Free Radical Biology and Medicine*, vol. 31, no. 4, pp. 509–519, 2001.

[32] S. Yang, D. Feskanich, W. C. Willett, A. H. Eliassen, and T. Wu, "Association between global biomarkers of oxidative stress and hip fracture in postmenopausal women: a prospective study," *Journal of Bone and Mineral Research*, vol. 29, no. 12, pp. 2577–2583, 2014.

[33] Q. Zhou, L. Zhu, D. Zhang et al., "Oxidative stress-related biomarkers in postmenopausal osteoporosis: a systematic review and meta-analyses," *Disease Markers*, vol. 2016, Article ID 7067984, 12 pages, 2016.

[34] S. A. Ahmed Amar, R. Eryilmaz, H. Demir, S. Aykan, and C. Demir, "Determination of oxidative stress levels and some antioxidant enzyme activities in prostate cancer," *The Aging Male*, vol. 22, no. 3, pp. 198–206, 2019.

[35] A. Djordjevic, S. Spasic, A. Jovanovic-Galovic, R. Djordjevic, and G. Grubor-Lajsic, "Oxidative stress in diabetic pregnancy: SOD, CAT and GSH-Px activity and lipid peroxidation products," *Journal of Maternal-Fetal and Neonatal Medicine: The Official Journal of the European Association of Perinatal Medicine, the Federation of Asia and Oceania Perinatal Societies, the International Society of Perinatal Obstetricians*, vol. 16, no. 6, pp. 367–372, 2004.

[36] F. L. Coe, E. M. Worcester, and A. P. Evan, "Idiopathic hypercalciuria and formation of calcium renal stones," *Nature Reviews Nephrology*, vol. 12, no. 9, pp. 519–533, 2016.

[37] N. S. Krieger, J. Asplin, I. Granja et al., "Chlorthalidone with potassium citrate decreases calcium oxalate stones and increases bone quality in genetic hypercalciuric stone-forming rats," *Kidney International*, vol. 99, no. 5, pp. 1118–1126, 2021.

[38] Z. Temova Rakusa, M. Pislar, A. Kristl, and R. Roskar, "Comprehensive stability study of vitamin D3 in aqueous solutions and liquid commercial products," *Pharmaceutics*, vol. 13, no. 5, p. 617, 2021.